Improving the performance of $Ge_2Sb_2Te_5$ materials via nickel doping: Towards RF-compatible phase-change devices

Pengfei Guo, Joshua A. Burrow, Gary A. Sevison, Aditya Sood, Mehdi Asheghi, Joshua R. Hendrickson, Kenneth E. Goodson, Imad Agha, and Andrew Sarangan

Citation: Appl. Phys. Lett. **113**, 171903 (2018); doi: 10.1063/1.5053713
View online: https://doi.org/10.1063/1.5053713
View Table of Contents: http://aip.scitation.org/toc/apl/113/17
Published by the American Institute of Physics

Improving the performance of $Ge_2Sb_2Te_5$ materials via nickel doping: Towards RF-compatible phase-change devices

Pengfei Guo,[1,a)] Joshua A. Burrow,[1] Gary A. Sevison,[1,2] Aditya Sood,[3,4] Mehdi Asheghi,[4] Joshua R. Hendrickson,[2] Kenneth E. Goodson,[4] Imad Agha,[1,5] and Andrew Sarangan[1,b)]
[1]*Department of Electro-Optics and Photonics, University of Dayton, Dayton, Ohio 45469, USA*
[2]*Air Force Research Laboratory, Sensors Directorate, Wright-Patterson AFB, Ohio 45433, USA*
[3]*Department of Electrical Engineering, Stanford University, Stanford, California 94305, USA*
[4]*Department of Mechanical Engineering, Stanford University, Stanford, California 94305, USA*
[5]*Department of Physics, University of Dayton, Dayton, Ohio 45469, USA*

(Received 24 August 2018; accepted 4 October 2018; published online 22 October 2018)

High-speed electrical switching of $Ge_2Sb_2Te_5$ (GST) remains a challenging task due to the large impedance mismatch between the low-conductivity amorphous state and the high-conductivity crystalline state. In this letter, we demonstrate an effective doping scheme using nickel to reduce the resistivity contrast between the amorphous and crystalline states by nearly three orders of magnitude. Most importantly, our results show that doping produces the desired electrical performance without adversely affecting the film's optical properties. The nickel doping level is approximately 2% and the lattice structure remains nearly unchanged when compared with undoped-GST. The refractive indices in amorphous and crystalline states were obtained using ellipsometry which echoes the results of X-ray diffraction. The material's thermal transport properties are measured using time-domain thermoreflectance, showing no change upon doping. The advantages of this doping system will open up opportunities for designing electrically reconfigurable high speed optical elements in the near-infrared spectrum. *Published by AIP Publishing.*
https://doi.org/10.1063/1.5053713

Amorphous-to-crystalline reversible phase transitions are found in many materials, most notably in chalcogenide glasses. This phase change, which is typically induced by heat, generated either using electrical current or optical excitation, results in very large changes in optical and electrical properties. These properties have been exploited in nonvolatile data storage devices such as rewritable digital versatile disks (DVD-RWs) and phase change random access memory devices (PCRAMs).[1–3] More recently, phase-change materials have been proposed as means for the phase and amplitude modulation of light,[4–6] exploiting the large index contrast between the amorphous and crystalline states. Among the various chalcogenide alloys, the pseudo-binary $Ge_2Sb_2Te_5$ (GST) has been widely studied because of its fast crystallization speed, reversible phase transition and good endurance over a wide temperature range. However, there are two primary challenges that limit the applications of GST in electronics, especially at high speeds such as in radio-frequency (RF)-compatible devices. The first is the extremely large resistivity in the amorphous state (several hundred Ωm). This necessitates either a large voltage, or a long (tens of ns) pulse, to dissipate sufficient power in the film to induce the phase transition. The second challenge is the large impedance difference between the amorphous and crystalline phases. In order to maintain a constant load impedance (nominally 50 Ω), one would have to utilize an impedance matching circuit with fast tunability, rendering the system nearly impractical for RF applications. Most of the work on modifying the GST electrical properties has so far been focused on reducing the switching current by increasing the resistivity of the GST in the amorphous state. Unfortunately, this also significantly increases the required voltage/switching time, which is especially important for quasi-static applications such as PCRAMs.[7]

During the past few years, different dopant elements have been explored for modifying the electrical and optical properties of GST as well as for improving its long-term stability. Previous work includes nitrogen,[8,9] carbon,[10,11] oxygen,[12] tin,[13] aluminum,[14] silver,[15] titanium,[16] tungsten,[17] and copper.[18] Although these studies showed that the resistivity of GST can be modified by adding dopants to the material, none have demonstrated the ability to reduce the resistivity of the amorphous state of the host GST material. Zhu *et al.*[19] studied nickel-doped GST with low nickel concentration (1% and 3%) for high speed phase change memory applications and improved data retention. While their work showed that 3% doping had a lower resistivity in the amorphous state and a higher resistivity in the crystalline state compared to undoped GST (whereas 1% doping showed almost no change), the optical properties and thermal conductivities were not examined in their work. These are important parameters for high-speed optical applications utilizing GST.

In this letter, we prepared 2% nickel-doped GST (hereafter, GST-Ni) films fabricated via co-sputtering. We examined a number of different properties of pure GST and GST-Ni films using energy dispersive X-ray spectroscopy (EDX), Raman spectroscopy, X-ray diffraction (XRD), time-domain thermoreflectance (TDTR), and ellipsometry. The aim of this work is to develop a nickel-doped GST platform suitable for high speed switching. Specifically, the goal is to show a path towards minimizing the impedance mismatch between the

[a)]Electronic mail: guop01@udayton.edu
[b)]Electronic mail: asaragan1@udayton.edu

amorphous and crystalline states without compromising the usefulness of the material in optical devices. We demonstrate that by comprehensively studying the Ni-doping of GST and its effects on electrical, thermal and optical properties.

Nickel-doped GST samples were prepared by co-sputtering using dual 3-in. circular magnetron cathodes. During deposition, one cathode was supplied from a 13.56 MHz RF source (for GST) and another cathode was supplied by a DC source (for nickel). Prior to deposition, the substrates (silica glass for electrical, XRD, Raman and ellipsometry characterization and crystalline silicon for TDTR) were cleaned using acetone-methanol-isopropyl alcohol (AMI) to remove organic contaminations and dried with nitrogen gas. The substrates were then placed in the chamber and pumped down to a base pressure below 1 μTorr.

The RF discharge power on the GST target was maintained at 100 W, while the DC power on the nickel target was set to various levels, ranging from 300 W down to 75 W to reduce the nickel concentration in the deposited films. As shown in Table I, reducing the DC power on the nickel target had the expected effect of reducing the doping level. Concentrations were obtained by averaging the measured EDX compositions from three separate areas on each sample. However, since the power cannot be arbitrarily scaled down to very low levels without compromising the stability and the repeatability of the plasma, the smallest doping concentration achievable was around 10%. Therefore, a wire mesh mask was implemented to further reduce the nickel deposition rate. This mesh, placed between the substrate and the sputter target, helped reduce the deposition rate by condensing a fraction of incident nickel atoms on the mesh. Using the co-sputtering system in combination with this meshed shutter, we were able to reduce the concentration down to 2% (or even lower by using a finer mesh). The deposited film thickness was obtained by measuring the step height using a stylus profiler. The thickness of the films used for the electrical, Raman, XRD, and ellipsometry experiments was approximately 200 nm, while that for TDTR was 405 nm.

The resistivity of the films as a function of annealed temperatures was obtained by first annealing each GST and GST-Ni sample at a series of discrete temperatures between 25 °C and 350 °C and then measuring their sheet resistance values by using a four-point probe. The annealing process was performed by placing the film in direct contact with the hot plate (i.e., the film facing down towards the hot plate) under ambient conditions for 3 min and returning to room temperature for the measurement.

The resistivity curves of GST (red) and GST-Ni (blue) as a function of annealing temperature are shown in Fig. 1.

TABLE I. Different deposition conditions and the corresponding nickel concentration in GST-Ni films.

DC power (W)	Pressure (mT)	Concentration (%)
300	8	≈20
150	8	≈15
75	8	≈12
75	6	≈10
75 (with mesh)	6	≈2

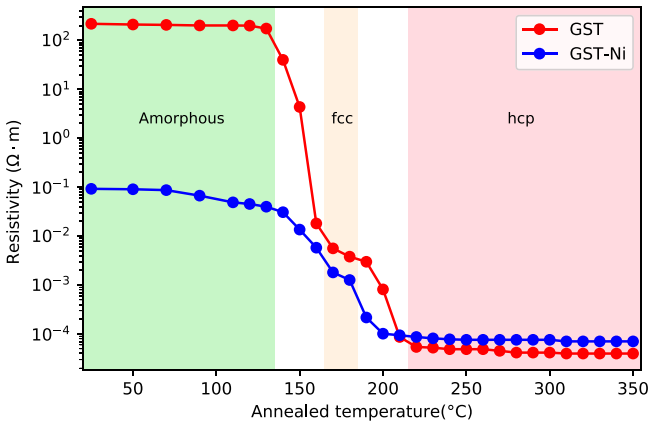

FIG. 1. Relationship between the resistivity and the annealing temperature of the as-deposited pure GST and GST-Ni (2%) films.

The resistivity of the GST films shows two discrete transitions. The first transition near 150 °C corresponds to the amorphous to face-centered-cubic (fcc) phase transition, while the second transition near 230 °C is due to the fcc to hexagonal close-packed (hcp) phase. On the other hand, the amorphous state resistivity of the GST-Ni film is lower than the undoped GST film by more than 3 orders of magnitude, while the resistivity in the crystalline states has comparable resistivity values (which is already highly conductive, and hence doping has little effect). In order to explain the decrease in resistivity of the amorphous state, we note that the atomic radius of Ni (135 pm) is close to that of Te (140 pm),[17] which makes it likely that nickel atoms act as substitutional impurities in the crystalline lattice of GST. In fact, similar substitutional effects of tungsten[17] and indium[20] in doped GST have been previously reported. As such, it is likely that nickel acts as an acceptor for germanium, making it a p-type dopant. To verify this hypothesis, we measured the electrical polarity of the films using the hot probe method.[21] The undoped GST films exhibited a p-type behavior, which is consistent with the report of Kato and Tanaka.[22] Even after nickel-doping, the films remained dominantly p-type. Furthermore, since the doped GST films exhibited a higher conductivity than the undoped GST films, this suggests that nickel atoms act as additional acceptor sites in the GST crystal lattice.

The structural information of the films related to their crystallization behaviors was obtained by characterization by XRD. The scanning range of diffraction angles is from 15° to 65°. Figure 2 shows the XRD patterns of the as-deposited GST and GST-Ni films after annealing them at 180 °C, 250 °C, and 350 °C, respectively. Since there are no identifiable peaks in the XRD patterns of the as-deposited films, we confirm that all the as-deposited films are in the amorphous state. The undulance around 29° may be due to the [200] peak.[23] After annealing the samples at 180 °C, both the GST and GST-Ni films crystallized into the metastable fcc state shown by the XRD peaks [111][2,22] and [222], which are typical for the NaCl-like cubic cell structure.[6] After both samples are annealed at 350 °C, new XRD peaks appear that correspond to the hexagonal state.[24] The Ni-doped GST shows lower XRD peak intensities, which indicate a lower crystallinity compared to pure GST. However, the diffraction

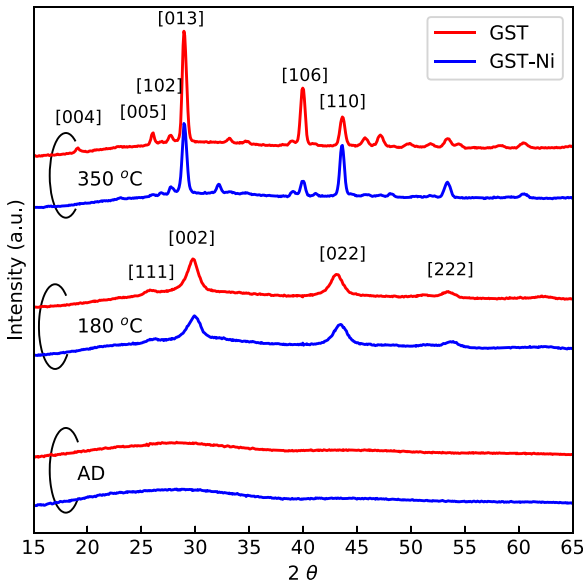

FIG. 2. XRD spectra of GST and GST-Ni samples for the as-deposited state (bottom) and after annealing at 180 °C (middle) and 350 °C (top). The curves have been offset for clarity.

peaks of both the samples are well aligned, which confirms that the small amount of nickel (2% in this case) does not significantly change the lattice structure of the host material.

To investigate the impact of nickel-doping on the short-range order of the films, we acquired the Raman spectra for GST and GST-Ni samples after annealing them at temperatures between 25 °C and 300 °C, as shown in Fig. 3. Both the undoped-GST and GST-Ni films exhibit two broad peaks around 65 cm^{-1} and 155 cm^{-1} in the as-deposited

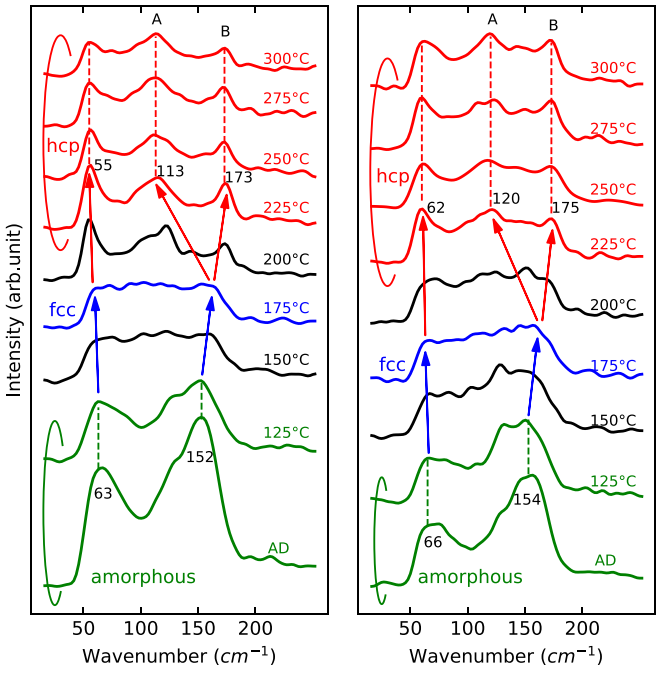

FIG. 3. Temperature dependence of Raman spectra of GST (left) and GST-Ni (right) from the as-deposited amorphous state to the hcp crystalline state after annealing at 300 °C. The vertical green and red dashed lines indicate the peak position in amorphous and hcp crystalline states, respectively. The solid arrows denote for peak shifting during phase transition. The black curves represent mixed transition states. All curves have been offset for clarity.

(amorphous) state. The peak near 65 cm^{-1} is related to a bending mode of $GeTe_4$, while the peak at 155 cm^{-1} is most likely due to a mode of $GeTe_4$ edge-sharing vibration. After annealing at 175 °C, both films show a broad band in the fcc state. From 175 °C to 225 °C, the peak at the larger wave number separates into two peaks, which are labeled as peak A (at a lower wave number, 120 cm^{-1}) and peak B (at a higher wave number, 175 cm^{-1}). Peak A is due to a vibration bond in $GeTe_4$ and/or pyramidal $SbTe_3$, while peak B corresponds to the Sb-Sb vibration mode. Beyond 225 °C, none of the peaks shows any further discernible changes, indicating that the film is fully crystallized and stabilized in the hexagonal state. In fact, these measurements echo the amorphous-fcc and fcc-hcp transitions from the resistivity plot in Fig. 1. The assignment of different Raman peaks can be inferred from several prior works on this topic.[17,25] Most importantly, our results show that the Raman spectra of GST and GST-Ni have similar characteristics throughout the entire phase transition temperature range, suggesting that there are no dramatic changes to the GST crystal matrix as a result of nickel doping.

Since phase change is a primarily thermal phenomenon, it is important to understand the effect of nickel doping on the thermal transport characteristics of the switching material. TDTR is an ultrafast optical pump-probe technique that is used to measure the thermophysical properties of thin films down to a few tens of nanometers in thickness. Details of this method and our setup are provided elsewhere.[26,27] Briefly, 9 ps pump pulses (532 nm wavelength) are used to heat the surface of the sample (405 nm thick GST on crystalline Si) through optical absorption within a thin 85 nm Al transducer layer. GST and GST-Ni materials are both in the amorphous state during all TDTR measurements. Time-delayed probe pulses (1064 nm wavelength), arriving 100 ps to 3 ns after the pump pulses, measure the rate of cooling of the metal layer as heat diffuses downwards into the GST film and the Si substrate, by monitoring changes in its reflectivity. These data are fit to the solution of a 3D heat diffusion model to extract the unknown thermophysical properties of interest within the film stack. The properties of the Al layer and the Si substrate are measured independently or taken from literature. The measurement is largely insensitive to the thermal boundary conductance at the Al/GST and GST/Si interfaces; each fixed at 100 $MW\,m^{-2}K^{-1}$ during the fitting. The volumetric heat capacity of GST is taken to be 1.4 $J\,cm^{-3}K^{-1}$ based on literature estimates[28] and assumed to be the same for the GST-Ni sample. In these measurements, we used a root mean square spot size ($1/e^2$ diameter) of 8.8 μm, and optical powers of 11 and 3 mW for the pump and the probe, respectively. The pump pulses were amplitude modulated at 10 MHz for lock-in detection. Representative TDTR time-decay curves for the GST and GST-Ni samples are shown in Fig. 4. From these, we extract a thermal conductivity of $0.21 \pm 0.03\,W\,m^{-1}K^{-1}$ for both samples, which is in good agreement with the literature for amorphous GST.[26,29] Importantly, we find that within the experimental uncertainties of the measurement, there is no detectable change in the thermal conductivity of GST due to 2% Ni doping.

For optical device applications of GST, such as switchable on-chip spatial light modulators, the most important

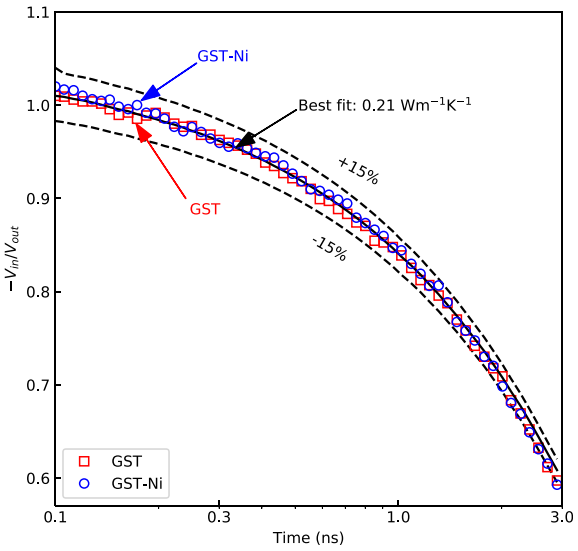

FIG. 4. Representative TDTR data for GST (red squares) and GST-Ni (blue circles) films. The black solid line denotes the best fit thermal conductivity of 0.21 W m^{-1} K^{-1}. Black dashed lines correspond to ±15% error bounds.

parameter is the refractive index contrast between the amorphous and crystalline states of GST. If doping is utilized to reduce the resistivity contrast to enable better electrical impedance matching, it is important to verify that this is not done at the expense of the refractive index contrast between the two states. To examine this, spectroscopic ellipsometry was used to study the refractive index and extinction coefficients of GST and GST-Ni thin films in both the amorphous and hcp crystalline states. The results are plotted in Fig. 5. The undoped GST is shown by red lines and the nickel-doped GST are shown by the blue lines. The solid curves represent the amorphous state (indicated by a-) and the dashed curves represent the hcp crystalline state (indicated by c-). In the wavelength range of interest, the refractive index n of both GST and GST-Ni increases by about 2 after the amorphous-to-crystalline transition, while the extinction coefficient κ increases by about 1, which is consistent with prior results.[6] The inset plots show the same data over a much larger spectral range. We can conclude from this data that nickel doping has not adversely affected the optical constants of GST, despite the dramatically altered electrical resistivity.

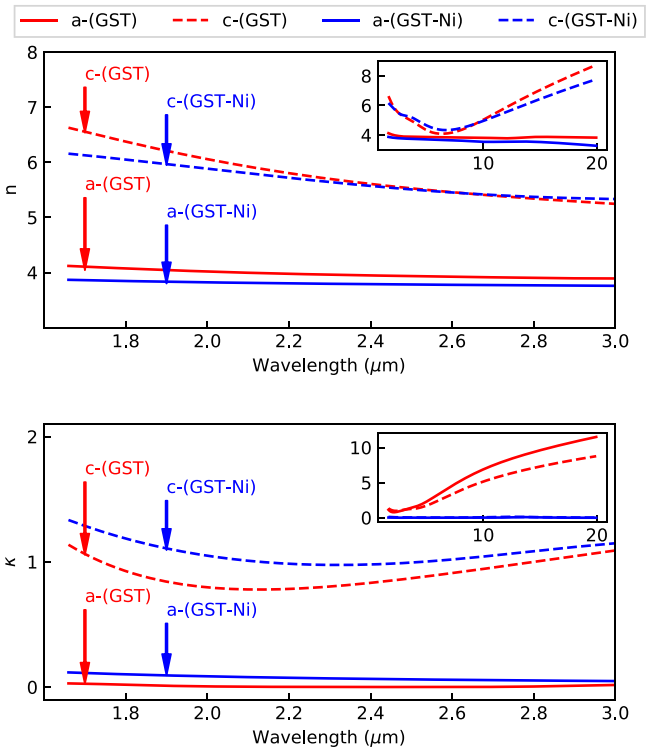

FIG. 5. Measured refractive index (top) and extinction coefficient (bottom) of GST and GST-Ni films in amorphous and crystalline states. The insets show n and κ in the spectrum up to 20 μm.

In summary, in this letter, we have carried out a comprehensive study of the effects of nickel doping in GST films pertaining to their electrical, structural, thermal, and optical properties. The resistivity of GST-Ni in the amorphous state was reduced by over 3 orders of magnitude as compared to the undoped GST, while the resistivity of the crystalline states remained nearly the same. This enables the fabrication of devices that can be readily impedance matched to high speed electronics irrespective of the actual GST state. The XRD and Raman spectroscopy results shows that the nickel dopant does not significantly change the lattice structures of the GST host material in both the amorphous and crystalline states. Furthermore, TDTR measurements indicate that thermal properties are nearly identical pre- and post-doping. More importantly, our ellipsometry results demonstrate that the refractive index contrast is well preserved and nickel doping does not adversely affect the optical constants in either amorphous or crystalline states. These results indicate that GST-Ni is a promising candidate for high-speed RF-compatible electrically switchable optical devices.

This work was supported by the National Science Foundation under Grant Nos. 1710273 and 1709200 and the University of Dayton graduate school. The authors thank Rachel H. Rai from the Department of Chemical and Materials Engineering at the University of Dayton for Raman measurements and Heungdong Kwon from the Department of Mechanical Engineering at Stanford University for inputs on TDTR measurements.

[1]J. H. Yi, Y. H. Ha, J. H. Park, B. J. Kuh, H. Horii, Y. T. Kim, S. O. Park, Y. N. Hwang, S. H. Lee, S. J. Ahn, S. Y. Lee, J. S. Hong, K. H. Lee, N. I. Lee, H. K. Kang, U.-I. Chung, and J. T. Moon, in *International Electron Devices Meeting* (2003), pp. 37.3.1–37.3.4.
[2]S. L. Cho, J. H. Yi, Y. H. Ha, B. J. Kuh, C. M. Lee, J. H. Park, S. D. Nam, H. Horii, B. K. Cho, K. C. Ryoo, S. O. Park, H. S. Kim, U.-I. Chung, J. T. Moon, and B. I. Ryu, in *Symposium on VLSI Technology* (2005), pp. 96–97.
[3]J. Lee, S. Choi, C. Lee, Y. Kang, and D. Kim, Appl. Surf. Sci. **253**, 3969 (2007).
[4]A. Karvounis, B. Gholipour, K. F. MacDonald, and N. I. Zheludev, Appl. Phys. Lett. **109**, 051103 (2016).
[5]J. Hendrickson, H. Liang, R. Soref, and J. Mu, Appl. Opt. **54**, 10698 (2015).
[6]A. Sarangan, J. Duran, V. Vasilyev, N. Limberopoulos, I. Vitebskiy, and I. Anisimov, IEEE Photonics J. **10**, 1 (2018).
[7]X. Dong, N. P. Jouppi, and Y. Xie, in *International Conference on Computer-Aided Design (ICCAD)* (IEEE, 2009), pp. 269–275.
[8]H. Seo, T.-H. Jeong, J.-W. Park, C. Yeon, S.-J. Kim, and S.-Y. Kim, Jpn. J. Appl. Phys., Part 1 **39**, 745 (2000).
[9]R. M. Shelby and S. Raoux, J. Appl. Phys. **105**, 104902 (2009).

[10]X. Zhou, L. Wu, Z. Song, F. Rao, M. Zhu, C. Peng, D. Yao, S. Song, B. Liu, and S. Feng, Appl. Phys. Lett. **101**, 142104 (2012).
[11]T. Li, L. Wu, X. Ji, Y. Zheng, G. Liu, Z. Song, J. Shi, M. Zhu, S. Song, and S. Feng, AIP Adv. **8**, 025201 (2018).
[12]S. Privitera, E. Rimini, and R. Zonca, Appl. Phys. Lett. **85**, 3044 (2004).
[13]M. L. Lee, K. T. Yong, C. L. Gan, L. H. Ting, S. B. M. Daud, and L. Shi, J. Phys. D: Appl. Phys. **41**, 215402 (2008).
[14]G. Wang, X. Shen, Q. Nie, R. Wang, L. Wu, Y. Lv, F. Chen, J. Fu, S. Dai, and J. Li, J. Phys. D **45**, 375302 (2012).
[15]C.-T. Lie, P.-C. Kuo, W.-C. Hsu, T.-H. Wu, P.-W. Chen, and S.-C. Chen, Jpn. J. Appl. Phys., Part 1 **42**, 1026 (2003).
[16]S. Wei, H. Zhu, K. Chen, D. Xu, J. Li, F. Gan, X. Zhang, Y. Xia, and G. Li, Appl. Phys. Lett. **98**, 231910 (2011).
[17]S. Guo, Z. Hu, X. Ji, T. Huang, X. Zhang, L. Wu, Z. Song, and J. Chu, RSC Adv. **4**, 57218 (2014).
[18]K. Ding, K. Ren, F. Rao, Z. Song, L. Wu, B. Liu, and S. Feng, Mater. Lett. **125**, 143 (2014).
[19]Y. Zhu, Z. Zhang, S. Song, H. Xie, Z. Song, X. Li, L. Shen, L. Li, L. Wu, and B. Liu, Mater. Res. Bull. **64**, 333 (2015).
[20]P. Lazarenko, A. Sherchenkov, S. Kozyukhin, A. Babich, H. Nguen, S. Timoshenkov, D. Gromov, A. Yakubov, and D. Terekhov, J. Phys. Conf. Ser. **690**, 012006 (2016).
[21]G. Golan, A. Axelevitch, B. Gorenstein, and V. Manevych, Microelectron. J. **37**, 910 (2006).
[22]T. Kato and K. Tanaka, Jpn. J. Appl. Phys., Part 1 **44**, 7340 (2005).
[23]S. Wei, J. Li, X. Wu, P. Zhou, S. Wang, Y. Zheng, L. Chen, F. Gan, X. Zhang, and G. Li, Opt. Express **15**, 10584 (2007).
[24]T. Matsunaga, N. Yamada, and Y. Kubota, Acta Crystallogr., Sect. B: Struct. Sci. **60**, 685 (2004).
[25]L. Bo, S. Zhi-Tang, Z. Ting, F. Song-Lin, and C. Bomy, Chin. Phys. **13**, 1947 (2004).
[26]C. Ahn, S. W. Fong, Y. Kim, S. Lee, A. Sood, C. M. Neumann, M. Asheghi, K. E. Goodson, E. Pop, and H.-S. P. Wong, Nano Lett. **15**, 6809 (2015).
[27]A. Sood, J. Cho, K. D. Hobart, T. I. Feygelson, B. B. Pate, M. Asheghi, D. G. Cahill, and K. E. Goodson, J. Appl. Phys. **119**, 175103 (2016).
[28]P. Zalden, K. S. Siegert, S. Rols, H. E. Fischer, F. Schlich, T. Hu, and M. Wuttig, Chem. Mater. **26**, 2307 (2014).
[29]H.-K. Lyeo, D. G. Cahill, B.-S. Lee, J. R. Abelson, M.-H. Kwon, K.-B. Kim, S. G. Bishop, and B.-K. Cheong, Appl. Phys. Lett. **89**, 151904 (2006).